Electronic Supplementary Information (ESI) for

Strain-modulated ferroelectricity and ferromagnetism in two-dimensional multiferroics of $CuCrP_2X_6$ (X = S, Se)

Yuxin Yang[a], Baojuan Xin[*a, b], Kaixin Zou[a], Zhixue Tian[c], Peizhen Hong[a], Hong Dong[a], Yahui Cheng [a], Hui Liu[a], Feng Lu[a], Wei-Hua Wang[*a]

[a]*Department of Micro/Nano Electronics, Tianjin Key Laboratory of Efficient Utilization of Solar Energy, Engineering Research Center of Thin Film Optoelectronics Technology (Ministry of Education), Nankai University, Tianjin 300350, China*

[b]*School of Integrated Circuits, Ludong University, Yantai 264025, China*

[c]*College of Physics, Hebei Key Laboratory of Photophysics Research and Application, Hebei Normal University, Shijiazhuang 050024, China*

*E-mail: whwangnk@nankai.edu.cn, bjxin@ldu.edu.cn

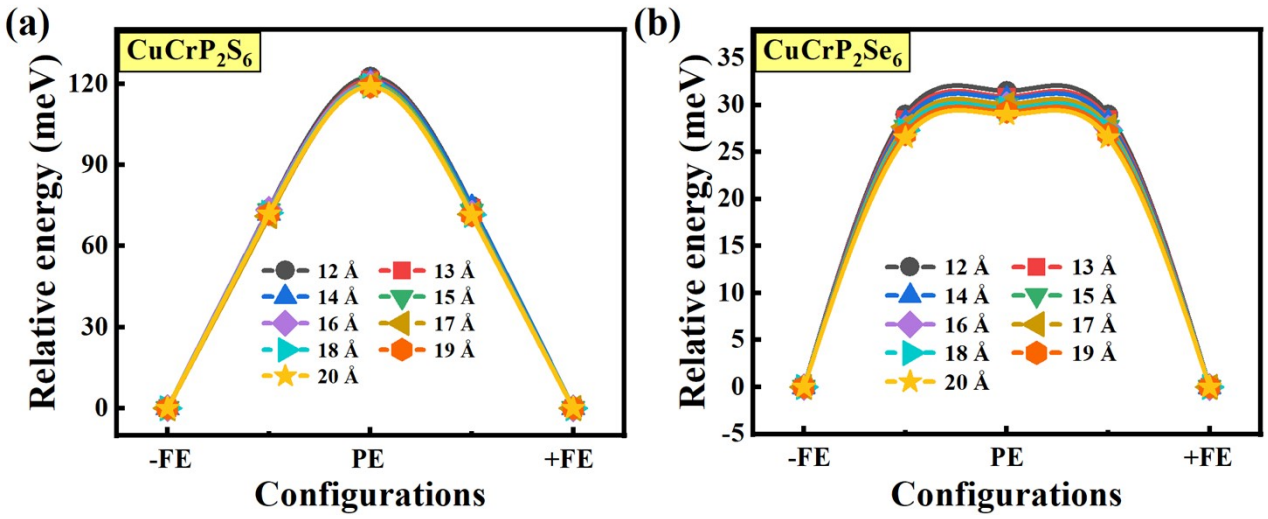

Fig. S1. The energy differences between the ferroelectric (FE) and paraelectric (PE) phases in (a) $CuCrP_2S_6$ and (b) $CuCrP_2Se_6$ monolayers under different vacuum thickness.

Table S1. The FE polarization and deviation of $CuCrP_2X_6$ monolayers obtained through three methods

	Berry phase	Charge density integration	Born effective charge	Deviation
$CuCrP_2S_6$	1.25 μC/cm^2	1.19 μC/cm^2	1.20 μC/cm^2	<5%
$CuCrP_2S_6$	1.11 μC/cm^2	1.06 μC/cm^2	1.08 μC/cm^2	<5%

The total out-of-plane FE polarization is the sum of out-of-plane ion polarization and out-of-plane electron polarization. The ion polarization is calculated by the point charge model. The effective dipole moment m_{el} of out-of-plane electron polarization can be deduced from the screening charge density as: $m_{el} = \int_{-\infty}^{+\infty} \Delta\rho(z) z dz$, where the planar averaged charge density $\rho(z)$ can be obtained by integration of the microscopic charge density $\rho(r)$ over the surface area A as $\rho(z) = \frac{1}{A}\iint \rho(r)dxdy$ and screening charge density $\Delta\rho(z)$ corresponds to the planar-averaged charge density difference between FE and PE phases: $\Delta\rho(z) = \rho(z)_{FE} - \rho(z)_{PE}$. After integration of $\Delta\rho(z)$, the out-of-plane FE polarization can be determined. Additionally, the FE polarization can be estimated via $P = \frac{1}{V}\sum_i Z_i^* \cdot u_i$, where V is the effective cell volume, Z_i^* and u_i are Born effective charge and cation polar displacement, respectively. In summary, the dependence on periodicity can be eliminated by the two approaches described above, ensuring the accuracy of the FE polarization. The deviation among different methods is less than 5%, indicating the reliability of the conclusions regarding the FE polarization of $CuCrP_2X_6$ monolayers in this work.

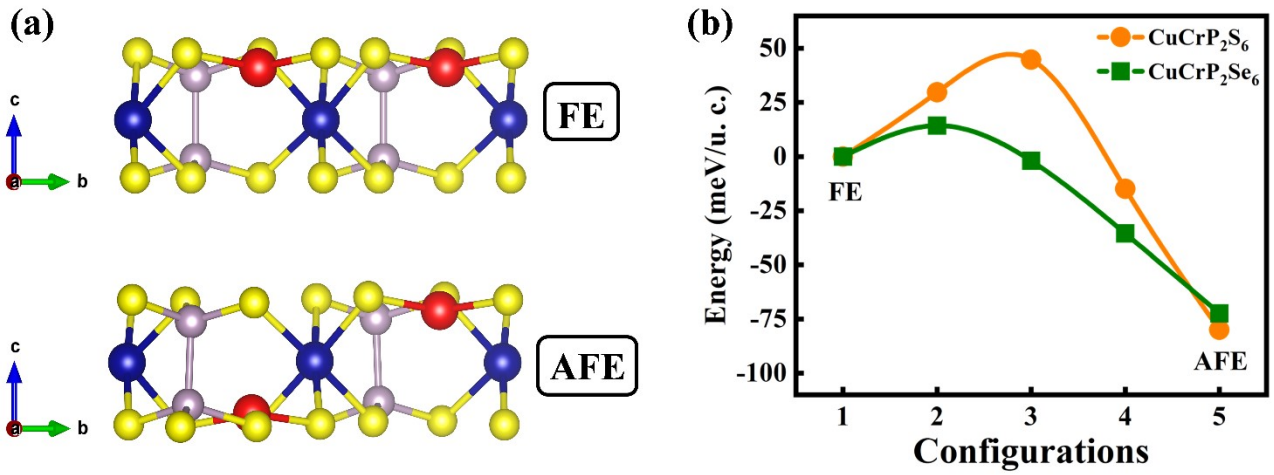

Fig. S2. (a) Side views of the FE and antiferroelectric (AFE) phases in $CuCrP_2X_6$ monolayers. (b) Energy barriers curves between the FE and AFE phases of $CuCrP_2X_6$ monolayers.

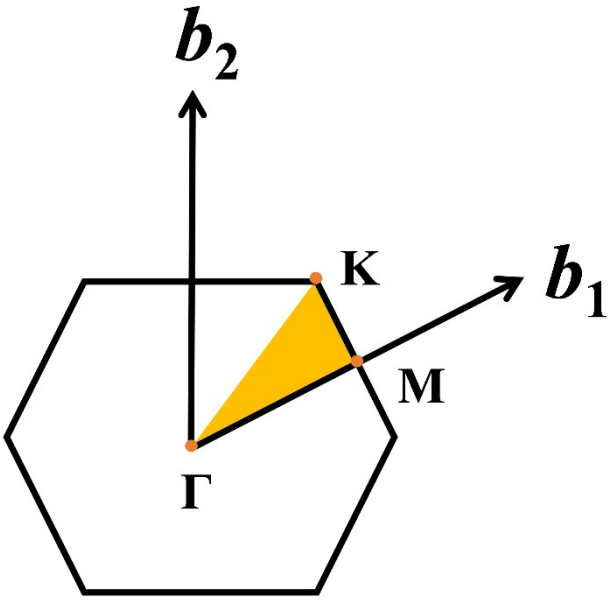

Fig. S3. The 2D Brillouin zone and high-symmetry *k*-points.

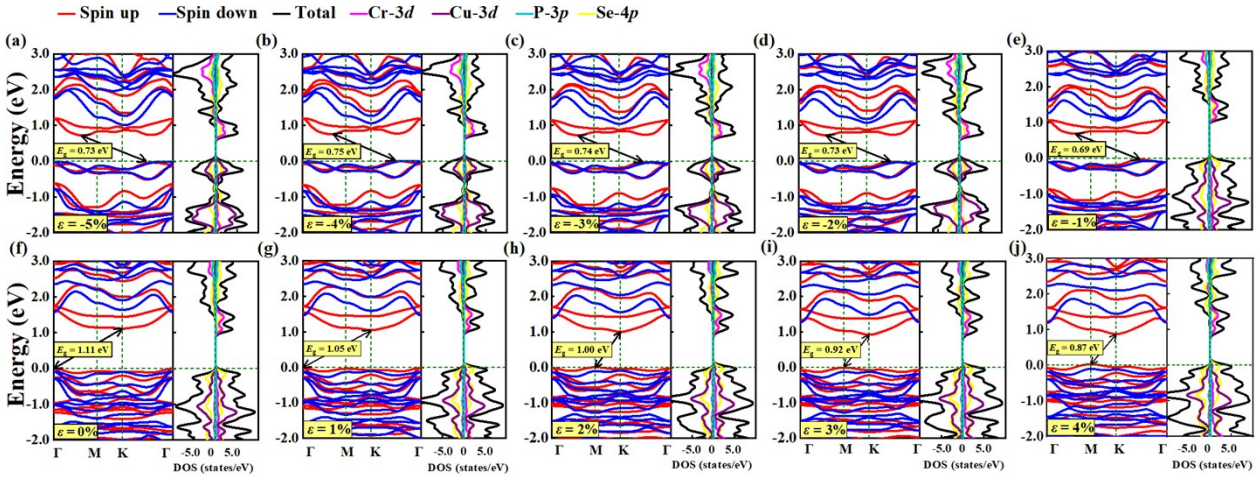

Fig. S4. Band structures and density of states of monolayer $CuCrP_2Se_6$ under biaxial strain. The biaxial strains are labeled by taking the fully relaxed lattice constant as the reference zero value. The Fermi level is indicated by a dashed green horizontal line, set to 0.0 eV. Black arrow connects the conduction band minimum (CBM) and the valence band maximum (VBM).

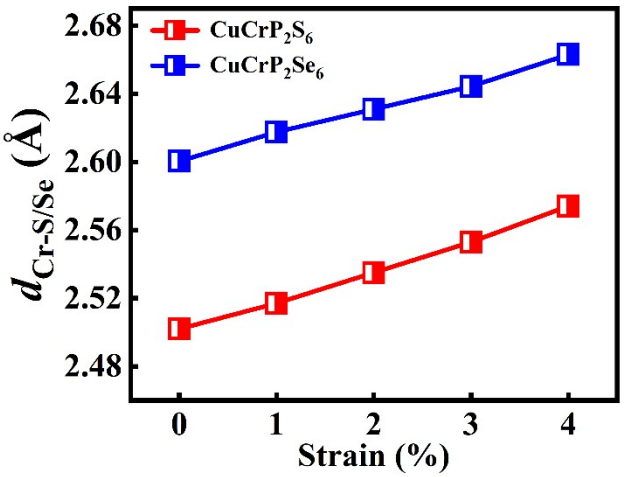

Fig. S5. The Cr-S/Se bond lengths in $CuCrP_2X_6$ monolayers under biaxial tensile strain.

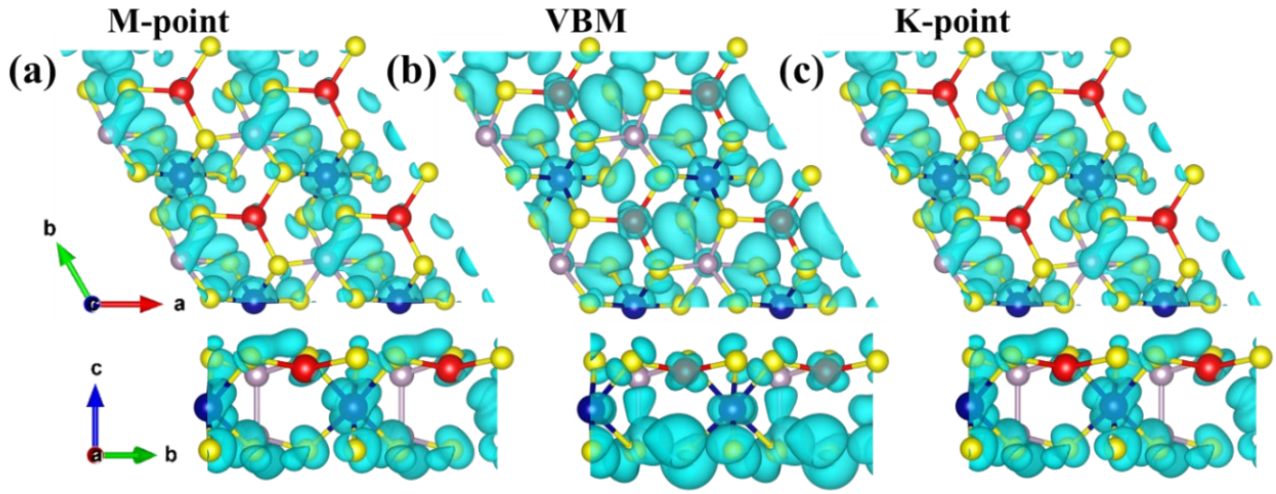

Fig. S6. Partial charge distribution images in (a) M-point of CBM, (b) VBM and (c) K-point of CBM for monolayer $CuCrP_2S_6$, respectively. The iso-surface value is set as 0.01 e/Å^3. Yellow, pink, blue, and red spheres represent the S atoms, P atoms, Cr atoms, and Cu atoms, respectively.

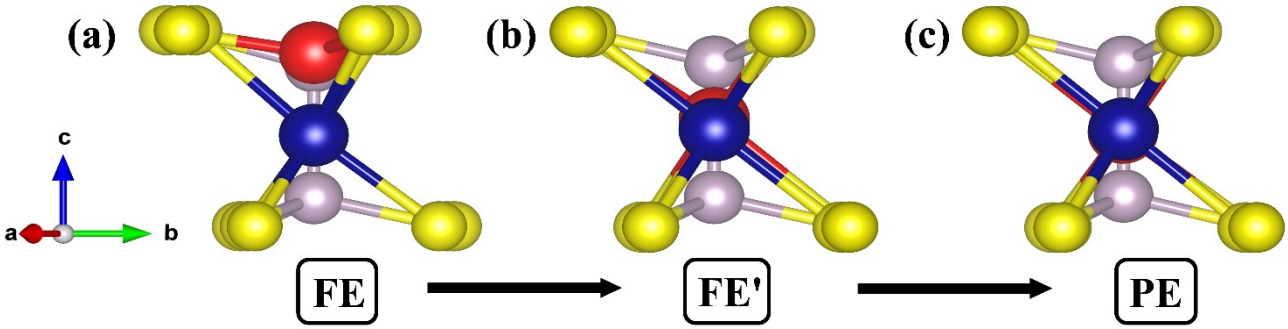

Fig. S7. The phase evolution of $CuCrP_2X_6$ monolayers under biaxial compressive strain.

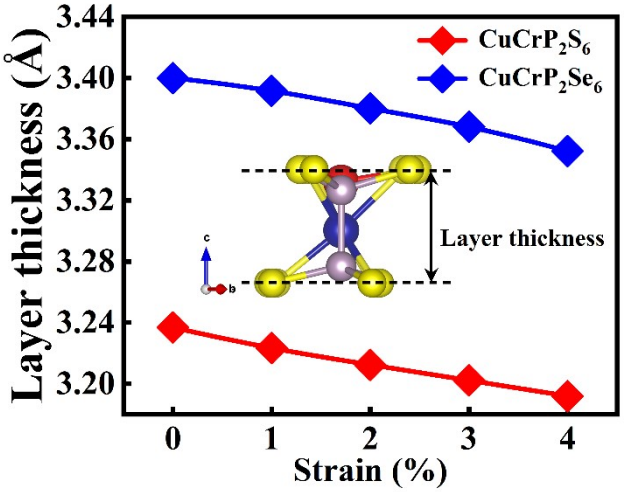

Fig. S8. The effective layer thickness in $CuCrP_2X_6$ monolayers under biaxial tensile strain.

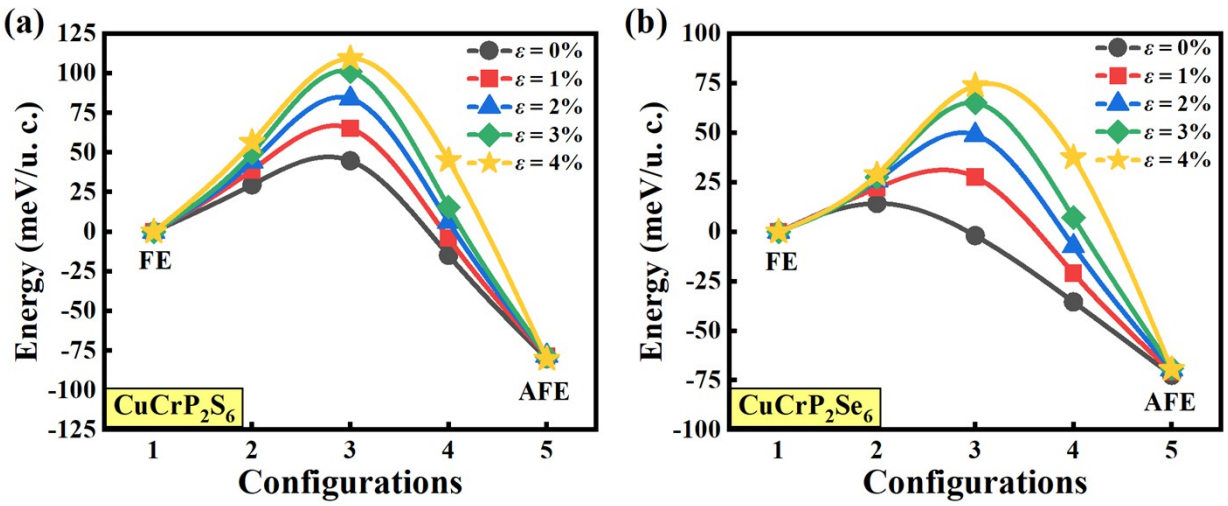

Fig. S9. The energy barriers curves between the FE and AFE phases in (a) $CuCrP_2S_6$ and (b) $CuCrP_2Se_6$ monolayers under biaxial tensile strain.

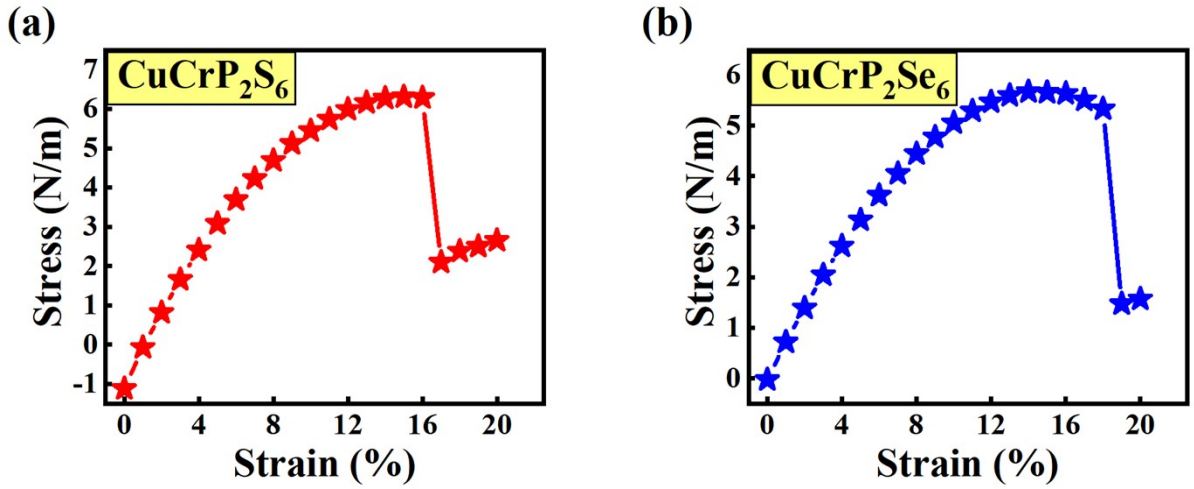

Fig. S10. The stress-strain curves in (a) $CuCrP_2S_6$ and (b) $CuCrP_2Se_6$ monolayers under biaxial strain, respectively. The unit of stress here is due to the simplification of the ultra-thin thickness of the 2D material, and its physical meaning should be clearly expressed as a line stress rather than a standard stress.

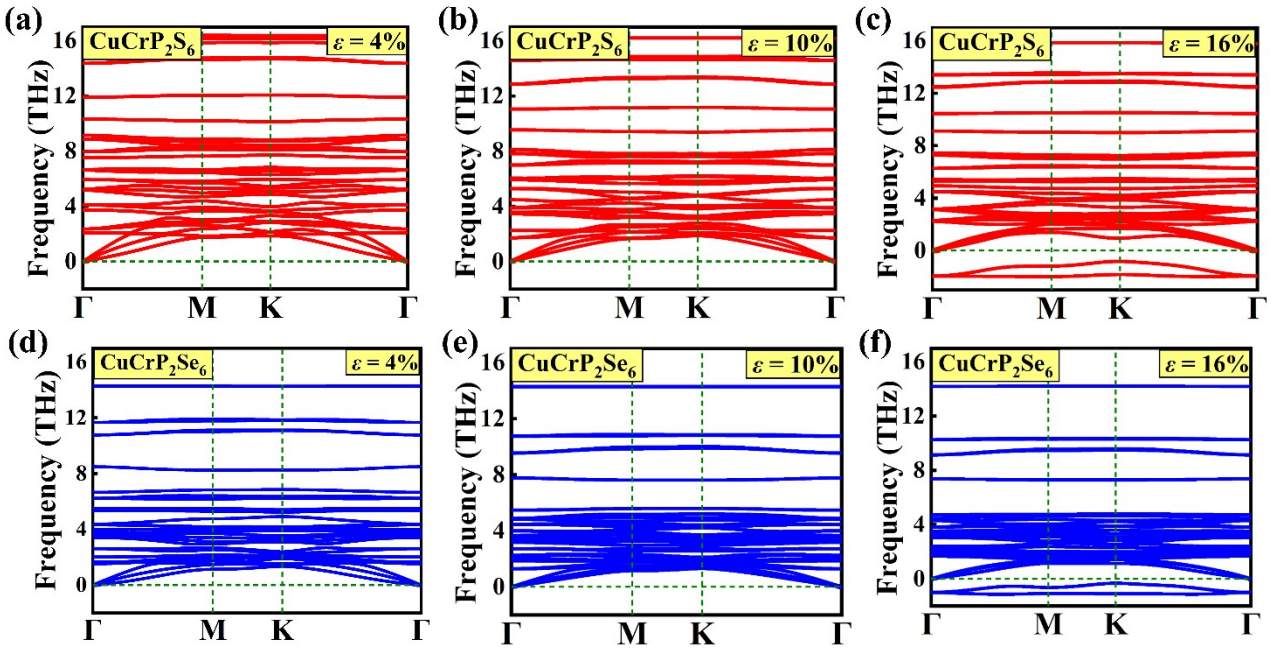

Fig. S11. The phonon spectra of $CuCrP_2X_6$ monolayers under biaxial tensile strain.

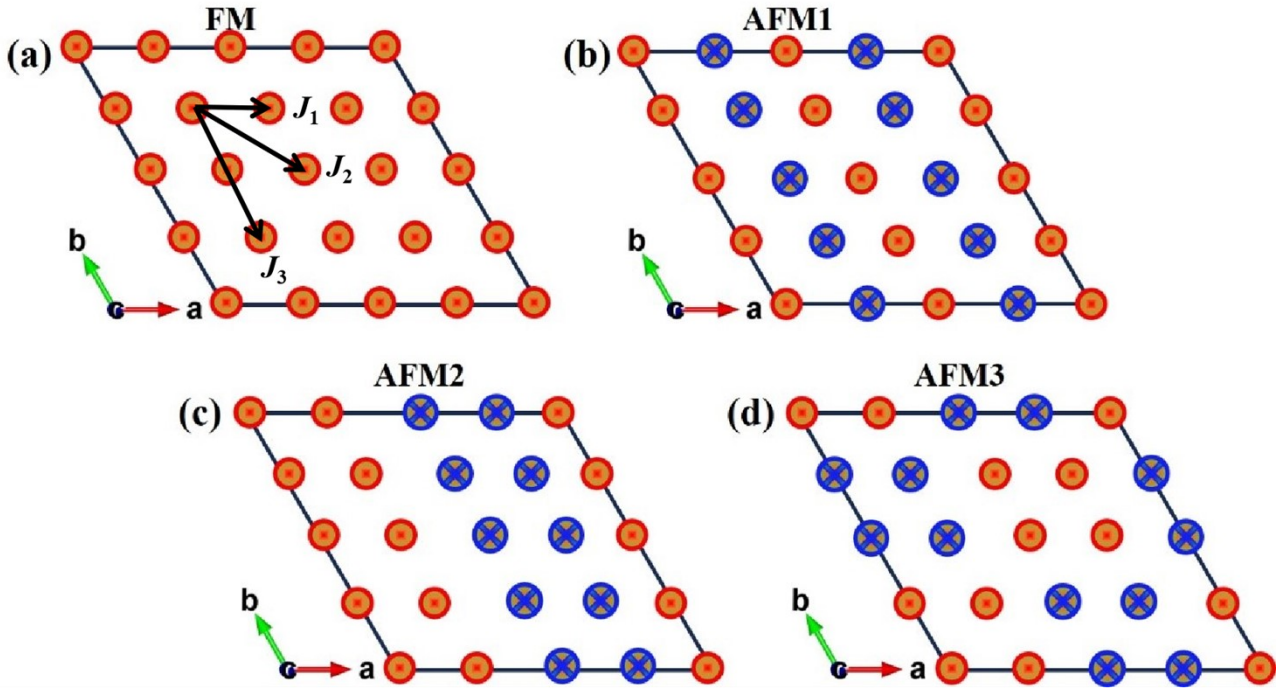

Fig. S12. The four possible magnetic configurations in $CuCrP_2X_6$ monolayers. The ball with a red point indicates the Cr atom with spin-up state, while the ball with a blue fork is the Cr atom with spin-down state. The J_1, J_2 and J_3 are the first, second and third nearest neighboring magnetic exchange coupling parameters, respectively.

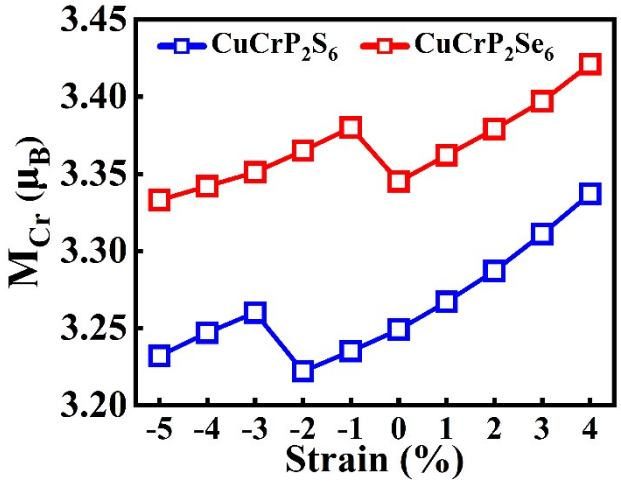

Fig. S13. The magnetic moments of Cr^{3+} cations in $CuCrP_2X_6$ monolayers under biaxial strain.

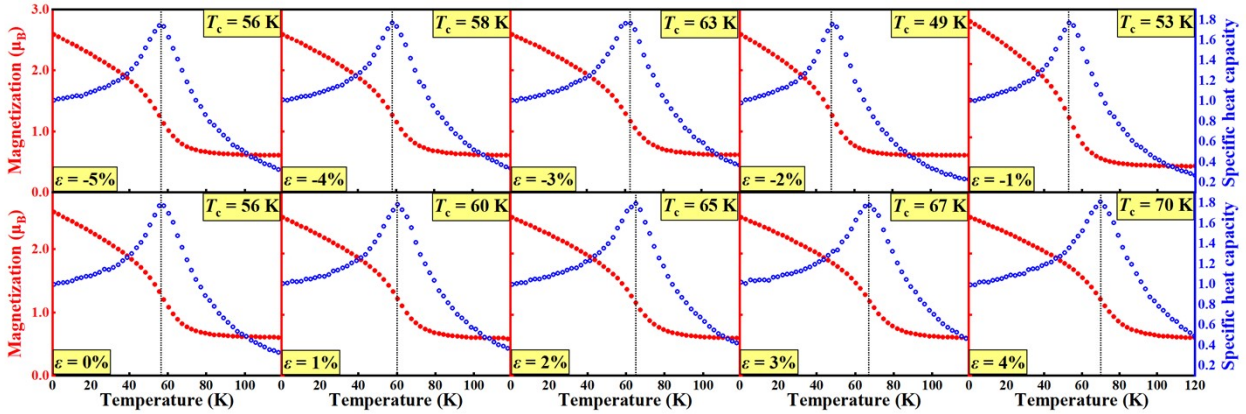

Fig. S14. The average magnetic moment (red line) and specific heat capacity (blue line) from Monte Carlo simulations for monolayer $CuCrP_2S_6$ under biaxial strain.

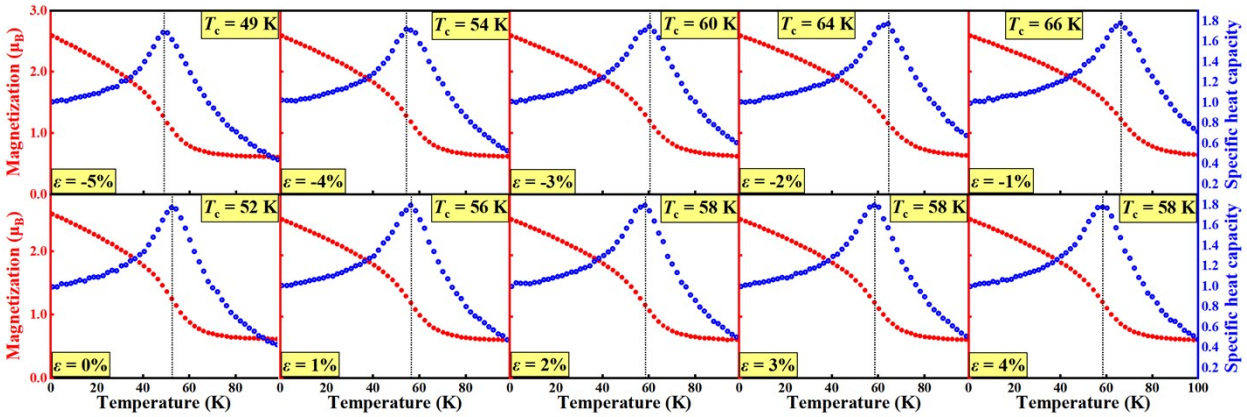

Fig. S15. The average magnetic moment (red line) and specific heat capacity (blue line) from Monte Carlo simulations for monolayer $CuCrP_2Se_6$ under biaxial strain.